CARNEGIE HUBBLE PROGRAM: A MID-INFRARED CALIBRATION OF THE HUBBLE CONSTANT

WENDY L. FREEDMAN[1], BARRY F. MADORE[1], VICTORIA SCOWCROFT[1], CHRIS BURNS[1], ANDY MONSON[1],
S. ERIC PERSSON[1], MARK SEIBERT[1], AND JANE RIGBY[2]

[1] Observatories of the Carnegie Institution of Washington, 813 Santa Barbara St., Pasadena, CA 91101, USA; wendy@obs.carnegiescience.edu,
barry@obs.carnegiescience.edu, vs@obs.carnegiescience.edu, cburns@obs.carnegiescience.edu, amonson@obs.carnegiescience.edu,
persson@obs.carnegiescience.edu, mseibert@obs.carnegiescience.edu
[2] Observational Cosmology Lab, NASA Goddard Space Flight Center, Greenbelt, MD 20771, USA; Jane.R.Rigby@nasa.gov

ABSTRACT

Using a mid-infrared calibration of the Cepheid distance scale based on recent observations at 3.6 μm with the *Spitzer Space Telescope*, we have obtained a new, high-accuracy calibration of the Hubble constant. We have established the mid-IR zero point of the Leavitt law (the Cepheid period–luminosity relation) using time-averaged 3.6 μm data for 10 high-metallicity, Milky Way Cepheids having independently measured trigonometric parallaxes. We have adopted the slope of the PL relation using time-averaged 3.6 μm data for 80 long-period Large Magellanic Cloud (LMC) Cepheids falling in the period range $0.8 < \log(P) < 1.8$. We find a new reddening-corrected distance to the LMC of 18.477 ± 0.033 (systematic) mag. We re-examine the systematic uncertainties in H_0, also taking into account new data over the past decade. In combination with the new *Spitzer* calibration, the systematic uncertainty in H_0 over that obtained by the *Hubble Space Telescope Key Project* has decreased by over a factor of three. Applying the *Spitzer* calibration to the *Key Project* sample, we find a value of $H_0 = 74.3$ with a systematic uncertainty of ± 2.1 (systematic) km s^{-1} Mpc^{-1}, corresponding to a 2.8% systematic uncertainty in the Hubble constant. This result, in combination with WMAP7 measurements of the cosmic microwave background anisotropies and assuming a flat universe, yields a value of the equation of state for dark energy, $w_0 = -1.09 \pm 0.10$. Alternatively, relaxing the constraints on flatness and the numbers of relativistic species, and combining our results with those of WMAP7, Type Ia supernovae and baryon acoustic oscillations yield $w_0 = -1.08 \pm 0.10$ and a value of $N_{\mathrm{eff}} = 4.13 \pm 0.67$, mildly consistent with the existence of a fourth neutrino species.

Key words: cosmological parameters – cosmology: observations – distance scale – galaxies: distances and redshifts – stars: variables: Cepheids

1. INTRODUCTION

Over the past several decades, there has been a steady increase in the accuracy with which extragalactic distances and the Hubble constant can be measured (e.g., Freedman et al. 2001, hereafter F01; Riess et al. 2011; Komatsu et al. 2011; and for a review see Freedman & Madore 2010). This has resulted from a number of factors: the availability, on the ground and especially in space, of high throughput, high dynamic range optical CCDs, and infrared arrays; the multi-wavelength sensitivity of these devices, making it possible to correct for systematic effects of reddening and metallicity; and using a wider range of methods for measuring relative distances beyond the immediate reach of Cepheid variables. Just over a decade ago, there was still debate over the value of the Hubble constant at a level of a factor of two; today, there is the promise of measuring the Hubble constant to an accuracy better than 2%.

In combination with other constraints (e.g., the angular power spectrum of cosmic microwave background anisotropies), an independent measurement of H_0 to accuracy of better than a few percent can provide critical constraints on the dark energy equation of state, the spatial curvature of the universe, neutrino physics, and general relativity (see Suyu et al. 2012 for a recent discussion). In practice, an accurate value of H_0 provides a means of breaking the degeneracies among several cosmological parameters. For example, measurements of cosmic microwave background anisotropies yield well-determined values of the products of $\Omega_m h^2$ and $\Omega_b h^2$ (where Ω_m and Ω_b are the matter and baryon densities, respectively), but not the densities, or H_0 independently. There are other degeneracies between H_0 and the

equation of state, w_0, as well as its evolution, w_a; between H_0 and the number of relativistic neutrinos, N_{eff} and the sum of the masses of neutrinos; and between H_0 and σ_8, the fluctuation of matter on 8 Mpc scales (for recent discussions, see Dunkley et al. 2009; Komatsu et al. 2009). Hence, the motivation for measuring an independent value of H_0 accurately to a few percent has continued to increase.

As described in Freedman et al. (2011, hereafter F11), we have begun a new Carnegie Hubble Program (CHP), specifically designed to minimize and/or eliminate the remaining known systematics in the measurement of the Hubble constant using mid-infrared data from NASA's *Spitzer Space Telescope*. Here, we report on a newly derived value of the Hubble constant and its uncertainty, based on the first data acquired from this program for Cepheids in the Milky Way and the Large Magellanic Cloud (LMC). Our focus in this paper is primarily the zero point of the Cepheid extragalactic distance scale and a reassessment of the systematic error budget.

2. A NEW MID-INFRARED ZERO-POINT CALIBRATION OF THE HUBBLE CONSTANT

As discussed at length in F11, there are many advantages in acquiring 3.6 μm data compared to optical observations. The effects of reddening are decreased (e.g., $A_V/A(3.6\ \mu\mathrm{m}) \sim 15$ and $A(I)/A(3.6\ \mu\mathrm{m}) \sim 8$; see F11 and references therein). Metallicity effects are both theoretically predicted and empirically demonstrated to be smaller. In addition, the dispersion in the Leavitt law is known to be more than a factor of two smaller in the mid-infrared than in the V band. The CHP is designed
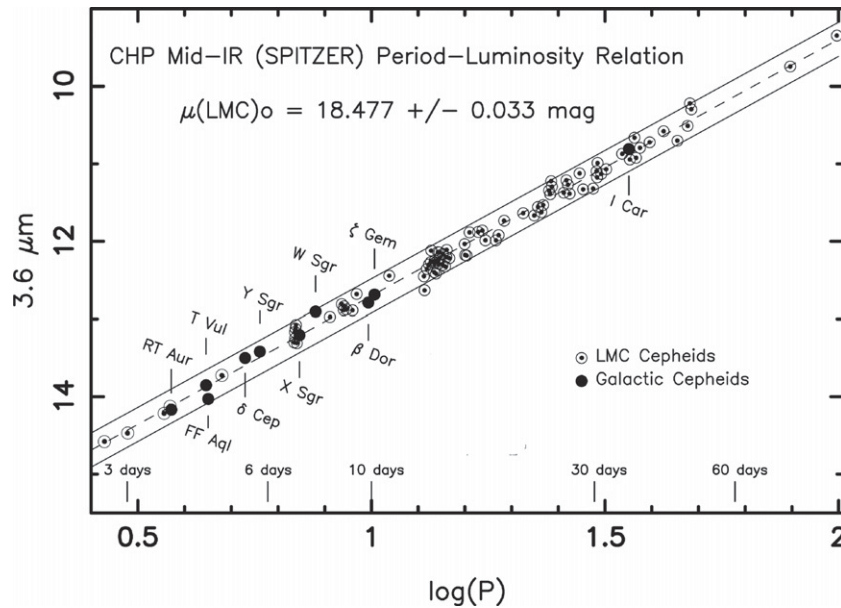
Figure 1. Leavitt law at 3.6 μm for 80 LMC Cepheids and 10 Milky Way Cepheids with *HST* trigonometric parallaxes. The Milky Way data are from Monson et al. (2012) and the LMC sample is from Scowcroft et al. (2012). The data have been corrected for extinction. Small circled points are LMC Cepheids; large filled circles, individually named, are Galactic Cepheids with trigonometric parallax measurements. The slope of the Leavitt relation is set by the LMC sample. Applying this slope to the Milky Way sample yields a reddening-corrected distance modulus of 18.477 mag to the LMC. The five LMC points with periods of less than six days are from the sample of Meixner et al. (2006). They are shown for illustration only and are not included in the fit to determine the slope. The dashed slope is defined by the sample of 80 LMC stars; the solid lines are 2σ ridge lines.

to establish the calibration of the Cepheid extragalactic distance scale at mid-infrared wavelengths by observing galaxies with known Cepheids in the Local Group and beyond, undertaking empirical tests for metallicity effects, and providing a mid-infrared calibration of the Tully–Fisher relation and for the Type Ia supernova (SN Ia) distance scale. The ultimate goal is a measurement of the Hubble constant to $\pm2\%$ (statistical plus systematic) uncertainty.

2.1. The CHP Data

To date, as part of the CHP, we have obtained 3.6 and 4.5 μm observations for a sample of 37 Galactic Cepheids (Monson et al. 2012), 10 of which have direct trigonometric parallaxes measured by the *Hubble Space Telescope* (*HST*) Fine Guidance Sensors (Benedict et al. 2007). Twenty-four observations were made at each wavelength for each Cepheid. Since the periods of these Cepheids are known a priori, we were able to schedule these 24 *Spitzer* observations with a roughly constant or uniform spacing over time for each of the stars. The Milky Way Cepheids range in period from roughly 4–36 days; 5 of these Cepheids have periods greater than 6 days. We have also obtained similarly high-quality, uniformly sampled data for 80 LMC Cepheids (Scowcroft et al. 2011, 2012), with periods in the range of 6–60 days, distributed across the face of the galaxy, and chosen to be relatively uncrowded, based on *H*-band images from Persson et al. (2004).

Although not originally designed for a cosmic distance scale program, *Spitzer* (Werner et al. 2004) has proven itself to be an excellent combination of telescope and instruments to measure the Cepheid distance scale at long wavelengths. The mid-IR Infrared Array Camera (Fazio et al. 2004) has the dynamic range, sensitivity, and the spatial resolution to be able to measure both the brightest of the Milky Way (calibrator) Cepheids and (with the same telescope, instrument, and filters) target and measure Cepheids in the LMC, as well as other nearby galaxies.

2.2. The Milky Way and LMC Leavitt (Cepheid Period–luminosity) Relations

Historically, the overlap in period between the Milky Way and LMC Cepheid calibrators has been small. Beyond the LMC, extragalactic distance scale measurements are necessarily limited to the brightest and longest-period Cepheids (generally $P > 10$ days.) The Galactic *HST* parallax sample contains only one truly long-period Cepheid, ℓ Car at $P = 35.5$ days. We therefore use the larger Cepheid sample in the LMC to define the slope and width of the long-period ($P \geqslant 6$ days) end of the Leavitt law. In Figure 1, we show the extinction-corrected Leavitt relations for the sample of 80 LMC stars with *Spitzer* data from Scowcroft et al. (2011, 2012). The 10 Milky Way calibrators with parallax measurements from Benedict et al. (2007) and new *Spitzer* observations from Monson et al. (2012)[3] are individually labeled. LMC data for stars with $P < 6$ days from Meixner et al. (2006) are also plotted, but not included in the fits. We note that the slopes of the mid-infrared Leavitt relations for both the Milky Way and the LMC are consistent over the entire period range from 4–60 days.

Both the slope and dispersion of the Galactic sample alone are, to within the measurement uncertainties, in agreement with the LMC Cepheid Leavitt relation. An unweighted least-squares fit to the 10 Milky Way stars from Monson et al. (2012) gives a slope of -3.40 ± 0.11, which is statistically in agreement with the more robust value (-3.31 ± 0.05) determined from the 80 stars covering the same period range in our LMC sample (Scowcroft et al. 2011, 2012). Table 8 of Monson et al. provides zero points and slopes for the 10 Milky Way Cepheids at 3.6 μm for a number of different weighting schemes, as well as a zero point obtained by fixing and adopting the LMC slope. The zero points are -5.81 (unweighted) and -5.80 (for two different

---

[3] We note that the photometry for two stars in Table 4 of Monson et al. has been updated by G. F. Benedict et al. 2012, private communication.

weighting schemes). For comparison, fixing the slope to be that for the LMC yields an intercept of −5.80 (unweighted) or −5.79 (weighted). In all cases, the computed uncertainty is 0.03–0.04, and the agreement is excellent.

The dispersion in the extinction-corrected Leavitt relation for the LMC at 3.6 μm amounts to only ±0.106 mag, giving an uncertainty of ±5% in distance for a single Cepheid; the dispersion for the sample of 10 Milky Way Cepheids is ±0.104 mag. Correcting for the tilt of the LMC (e.g., Scowcroft et al. 2012), the scatter in the 3.6 μm Leavitt relation reduces from ±0.106 to ±0.100 mag. With this sample of Cepheids observed at these long wavelengths, the random error on the distance modulus to the LMC has been reduced to ±0.100/$\sqrt{80}$ = ±0.011 mag. We take the systematic error on the distance modulus to the LMC to be defined by the uncertainty in the Milky Way best-fit intercept, when both the slope and the intercept are fit simultaneously for the 10 Milky Way Cepheids, given by ±0.104/$\sqrt{10}$ = 0.033 mag. Adopting the 10 Galactic calibrators, these data yield a true distance modulus to the LMC of 18.477 ± 0.011 (statistical) ±0.033 mag (systematic).

2.3. Applying the New Spitzer Calibration

Most recent extragalactic studies have used the distance to the LMC as fiducial. For example, the methodology of the *Key Project* (F01) was to adopt an LMC true distance modulus of 18.50 ± 0.10 mag and a reddening to the LMC of $E(B − V) = 0.10$ mag. Relative distance moduli of galaxies beyond the LMC were then determined using the reddening-free Wesenheit function, $W = V − R \times (V − I)$, where R is the ratio of total to selective absorption. The advantage of this approach is that given an updated zero point, any offset can simply be applied to the entire *Key Project* distance scale.

We apply our new *Spitzer* zero-point calibration to the Benedict et al. (2007) Milky Way parallax stars, and combine it with the *HST Key Project* data from F01. We note that the mid-IR *Spitzer*-based distance modulus for the LMC is 0.023 mag (∼1.2% in distance) smaller than the value of 18.50 mag adopted by F01 as part of the *Key Project*, thus increasing H_0 by 1.2%. In addition (as described in Section 3.2), switching from an LMC-based zero point to the Milky Way calibration, the metallicity correction to the *Key Project* sample is now also significantly reduced (by 0.04 mag giving an additional 2% increase in H_0). We obtain a value of $H_0 = 74.3 \pm 2.1$ (*systematic*) km s^{-1} Mpc^{-1}. This value of the Hubble constant is in excellent agreement with that of F01, as well as more recent determinations by Riess et al. (2011) and Komatsu et al. (2011). We provide a detailed discussion of the systematic uncertainty on this value in the following section.

3. DECREASING/ELIMINATING THE SYSTEMATICS

At the conclusion of the *Key Project*, F01 quantified the outstanding sources of *systematic* uncertainty (their Table 14) known to be affecting the value of the Hubble constant at that time. These included the absolute zero point of the Leavitt law, which was explicitly tied to the distance to the LMC (±5%); the uncertainty in the metallicity correction to the Leavitt period–luminosity (PL) relation, resulting from the systematic offset in mean metallicity between the LMC and many of the more distant (higher-metallicity) spiral galaxies (±4%); the cumulative uncertainties resulting from the cross-calibrating of instruments, filters, and detectors from the ground to space (±3.5%); systematic reddening errors (±1%); bias in fitting

the PL relation to truncated data (±1%); crowding or blending of images based on artificial star tests (0, +5%); and, finally, allowing for bulk flows on large scales (±5%).

The mid-infrared/trigonometric parallax calibration for Galactic Cepheids immediately solves two outstanding problems. It provides an accurate (geometric) foundation upon which to set the zero point of the Leavitt law, at any given wavelength. In addition, it provides high-metallicity Cepheid calibrators that are more comparable to the bulk of high-metallicity Cepheids in the target galaxies used for the *HST Key Project*, as well as other determinations of H_0.

Below, we discuss the two systematic errors for which there is significant quantitative improvement resulting from the new *Spitzer* data. We then discuss the status of other terms entering the systematic error budget.

3.1. Absolute Zero Point of the PL Relation

As we saw in Section 2, the measured scatter in the Milky Way Leavitt relation of ±0.104 mag suggests that the 10 Galactic calibrators define the zero point to ±0.104/$\sqrt{10}$ = 0.033 mag. We adopt this value as the systematic error on the zero point of the Cepheid PL relation. Despite the small sample of Galactic calibrators, the systematic error on the zero point of the Cepheid Leavitt relation is already reduced to only 1.7% in distance, i.e., a factor of three better than the quoted uncertainty of the *HST Key Project* zero point. This uncertainty is also a measure of the *systematic error* on the distance to the LMC.

We have been awarded further *Spitzer* time to observe a sample of nearby Galactic Cepheids, so that ultimately *Gaia* can provide accurate parallaxes for a sample size comparable to that of the LMC. Windmark et al. (2011) have recently discussed the potential of using *Gaia* to determine the Cepheid zero point. Although they estimate that approximately 9000 Cepheids will be within reach of *Gaia*, the overall accuracy will be limited by systematic effects, primarily reddening. Hence, obtaining mid-infrared observations for these Milky Way Cepheids remains critical.

3.2. Metallicity Dependence and Offsets

A number of observations and tests are built into the CHP *Spitzer* program (see F11) to quantify the magnitude of any residual metallicity effect. The first of these tests is discussed in F11, where the deviations of individual 3.6 μm LMC Cepheid magnitudes from the PL relation, as a function of spectroscopic [Fe/H] metal abundances (from Romaniello et al. 2008), exhibit only a very shallow (and statistically insignificant) slope of −0.09 ± 0.29 mag dex^{-1}. Moreover, Figure 7 of F11 shows no evidence of any metallicity effect for three Galactic Cepheids for which there are both 3.6 μm data and [Fe/H] measurements. As we noted above, in moving to a zero-point calibration of the Milky Way Cepheid PL relation at 3.6 μm, the Cepheid zero-point calibration can now be directly established at high metallicity, avoiding the intermediate step of calibrating with the (lower-metallicity) LMC.

The metallicities (12 + log (O/H)) of the LMC, Milky Way, and the mean of the *Key Project* spiral galaxies are 8.50, 8.70, and 8.84 dex, respectively (F01 and references therein; Allende-Prieto et al. 2001). For the *Key Project*, a slope of the metallicity correction of −0.20 ± 0.2 mag dex^{-1} was adopted, where 1 dex corresponds to a factor of 10 in metallicity. Specifically, a correction to the distance modulus of $\Delta\mu = −0.20 \times$ ([O/H]–[O/H]$_{LMC}$) was made. F01 adopted a metallicity correction of $−0.20 \times 0.34 = −0.068$ mag, corresponding
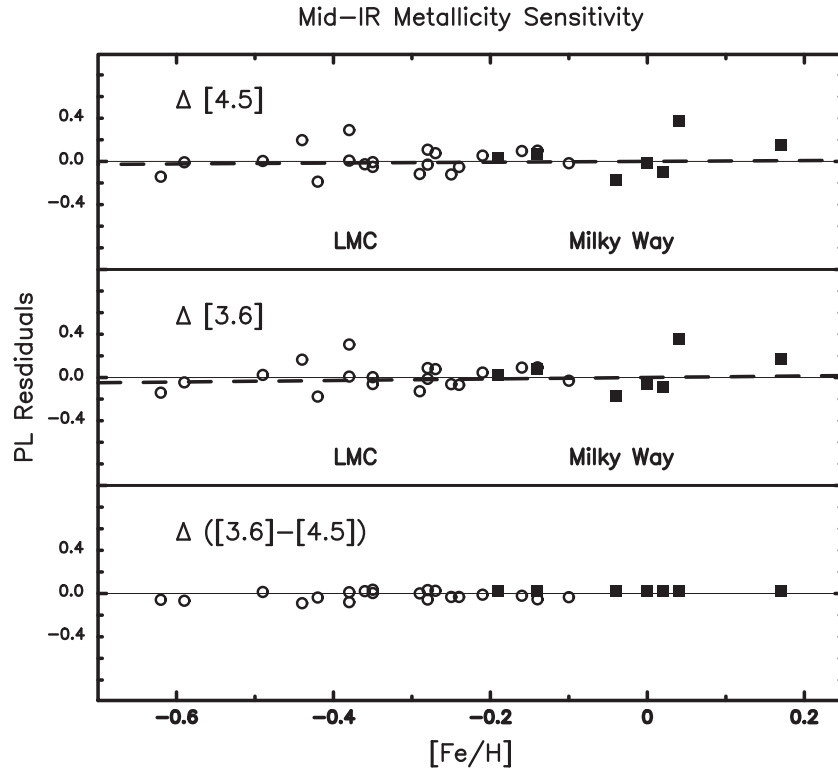
Figure 2. Sensitivity of mid-infrared Cepheid magnitudes to metallicity. The (lower-metallicity) Large Magellanic Cloud Cepheids are shown as open circles; the (higher-metallicity) Milky Way Cepheids are plotted as filled squares. The PL residuals are measured in the sense of observed magnitudes minus the mean PL relation. The highly correlated nature of the vertical scatter in these plots is a reflection of the scatter due to temperature and radius variations across the instability strip and to correlated back-to-front geometric effects. Neither of these effects are expected to correlate with metallicity. No statistically significant correlation of the Cepheid magnitudes with atmospheric [Fe/H] metallicity can be seen in these plots. The 4.5 μm residuals are plotted in the upper panel; the 3.6 μm residuals are shown in the middle panel. The lower panel shows the remarkably small scatter in the color residuals as a function of metallicity where the correlated scatter due to instability strip position and back-to-front geometry is canceled.

to a decrease in the Hubble constant of 3.5%, and adopted an uncertainty corresponding to the entire correction. Now, correcting back from the LMC to solar metallicity (0.20 mag dex^{-1} × 0.20 dex = 0.040 mag) results in a differential correction to the Hubble constant of +2%. In the past, we conservatively adopted the total magnitude of the correction as being equivalent to its own systematic uncertainty. The difference between the *Key Project* sample and the Milky Way now implies a correction of 0.2 mag dex^{-1} × 0.14 dex = 0.028 mag or 1.4% in the distance scale.

In Figure 2, we show updated and revised plots of magnitude and color residuals from the mid-IR PL relations plotted as a function of spectroscopic atmospheric [Fe/H] metallicities from Romaniello et al. (2008). This plot supersedes earlier versions given in Freedman & Madore (2010) and Freedman et al. (2011) as it now uses the final magnitudes and PL fits for the entire LMC sample given in Scowcroft et al. (2011, 2012) and extends the Milky Way sample to significantly higher metallicities using the newly published Galactic Cepheid mid-IR data of Monson et al. (2012). The formal solutions are $\Delta[3.6] = +0.07(\pm0.18)$ [Fe/H] $- 0.01(\pm0.06)$ and $\Delta[4.5] = +0.04(\pm0.19)$[Fe/H] $+ 0.04(\pm0.06)$. These data are consistent with no significant correlation between the metallicity and the 3.6 or 4.5 μm Cepheid magnitudes over the metallicity range $-0.6 <$ [Fe/H] $< +0.2$.

3.3. Other Systematic Effects

WFPC2 zero point/instrumental systematics. As discussed in Stetson (1998), the Wide Field and Planetary Camera 2

(WFPC2) on *HST* had an imperfect charge transfer efficiency. To quantify the uncertainties, Stetson carried out an extensive comparison of WFPC2 and ground-based photometry for Milky Way globular cluster stars. He found that the formal standard errors in this comparison were significantly less than 1%, but concluded that the true external uncertainties were more likely at least of the order of 1%. A difference of 0.07 ± 0.02 mag was found between the ground-based and WFPC2 photometry, and this correction was applied to the latter in F01. We note that in Table 14 of F01, the magnitude of this offset (0.07 mag or 3.5%) rather than the uncertainty (0.02 mag or 1%) was tabulated. In this paper, we quote the original uncertainty consistent with that determined by Stetson (1998).

Reddening. From the optical through the infrared, the effect of interstellar extinction is a generally declining function of increasing wavelength. A significant advantage of observing Cepheids in the mid-infrared is therefore a reduced sensitivity to extinction (both Galactic and extragalactic). The interstellar extinction law at mid-infrared wavelengths has now been measured by a number of authors (see F11 and references therein). The shape of the extinction curve shows some variation between different sight lines, with an observed range of $A_\lambda/A_V =$ 0.058 to 0.071 at 3.6 μm and 0.023–0.060 at 4.5 μm. However, the extinction measured in magnitudes in the mid-IR, as compared to optical *V*-band data, for example, is reduced by factors of 14–17 at 3.6 μm and 16–43 at 4.5 μm. Thus, moving to the mid-IR reduces, by more than an order of magnitude, the sensitivity of the zero point of the Cepheid distance scale to reddening corrections. Although uncertainties in reddening may contribute to statistical uncertainties (at the <1%
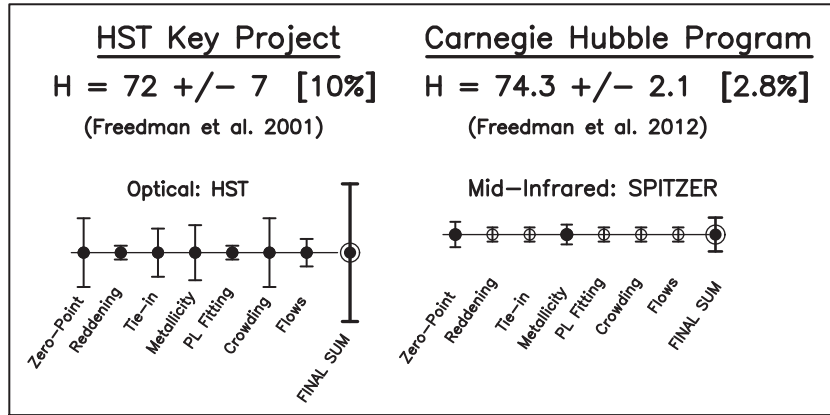
Figure 3. Comparison of the seven dominant sources of systematic error in determining the Hubble constant. The left-hand panel shows the individual errors given for the *HST Key Project* by Freedman et al. (2001) (filled circles), followed by the total systematic error formed from the quadrature sum of the six preceding values (circled dots). The right-hand portion of the panel shows the current errors for the same terms for the CHP determination of the Hubble constant. Open circles represent systematic terms that have estimated errors less than or equal to 1%. As discussed in Section 3, the sharp drop in the crowding error on the right-hand side is based on both the new simulations described in the Appendix, as well as the original analysis by Ferrarese et al. (2000). The lower error for the tie-in error results from correcting an error in Table 14 of Freedman et al. (2001), which reported the magnitude of a photometric zero-point correction and not its uncertainty. The decrease in the zero-point and metallicity uncertainties result from the new *Spitzer* data.

Table 1
CHP Dominant Systematic Uncertainties in H_0

Source	Uncertainty	Section/Description
Absolute zero point	1.7%	Section 3.1 new Milky Way parallaxes + *Spitzer*
Metallicity dependence	1.4%	Section 3.2 Milky Way as reference galaxy
WFPC2 zero point	1%	Section 3.3 ground-based tie-in
Crowding	1%	Section 3.3 artificial star tests
Large-scale flows	1%	Section 3.3 recent large-scale supernova and galaxy surveys

Notes. Final adopted value: $H_0 = 74.3 \pm 1.5$ (statistical) ± 2.1 (systematic) km s^{-1}Mpc^{-1}.
Percent error: [$\pm 2.0\%$]   [$\pm 2.8\%$].

level) for individual galaxies, as discussed in F01, they are no longer a significant contributor to the overall systematic error budget.

PL fitting bias. Apparent magnitude cutoffs in the discovery and measurement of Cepheids at the detection limits of surveys can, in principle, give rise to biased fitting errors. This effect is a decreasing function of width (i.e., intrinsic dispersion) of the PL relation, and hence is again ameliorated by working at mid-infrared wavelengths, or using the reddening-free magnitude, W. By performing successive period cuts, F01 determined that the bias was negligible for the *Key Project* sample, with the mean correction for the sample amounting to 0.01 mag. A period cut was applied to the shortest period Cepheids to correct for this small bias.

Crowding. At present, crowding is not an issue for the Milky Way Cepheids, which are bright and isolated. It is also not a significant issue for the LMC sample of Scowcroft et al. (2011, 2012), where the LMC sample Cepheids were pre-selected on the basis of near-infrared images to be isolated. In the case of the more distant *HST Key Project* sample, a published uncertainty of <0.02 mag ("even in the most problematic cases") was given by Ferrarese et al. (2000) based on artificial star tests. We note that F01 adopted an uncertainty of 5% (0.10 mag) due to crowding; however, no justification was provided for this larger adopted value, and the quantitative basis for this uncertainty relies on the artificial star experiments. In the Appendix, we further quantitatively explore the effects of crowding on Cepheids by blue main-sequence stars, and find, in agreement with the results of Ferrarese et al., that crowding effects in the mean are less than 1%.

Large-scale flows. Early cold dark matter models of large-scale structure (e.g., Turner et al. 1992) suggested that sparse sampling of cosmologically small volumes could give rise to biased values of the Hubble constant (at the 2%–4% level in samples only extending out to 10,000 km s^{-1}). For scales out to 40,000 km s^{-1}, variations were predicted to be only 1%–2%. Over time, the data constraining the local Hubble flow have continued to increase in sample size, depth, and precision. Recent analyses of a sample of well-measured SNe Ia (Hicken et al. 2009) sampling volumes with velocities extending to over 20,000 km s^{-1} suggest that there are no significant systematic departures of the Hubble constant from its globally averaged value; i.e., there is no local void. This is also consistent with the analysis of Sandage et al. (2010); see also Turnbull et al. (2011) and references therein for a recent discussion of bulk flows. At present, we conservatively include a 1σ systematic error of 1% for large-scale flows.

3.4. Summary of Systematic Effects

We summarize our adopted systematic errors for H_0 in Table 1. The errors are also displayed graphically in Figure 3 and compared with those from the *HST Key Project*. The current dominant source of systematic uncertainty remains the absolute zero point; however, this uncertainty is a factor of three smaller than for the *HST Key Project* results of a decade ago. Adding the individual contributions in Table 1 in quadrature yields an overall systematic uncertainty of ± 2.1 km s^{-1} Mpc^{-1} or an uncertainty of 2.8% for $H_0 = 74.3$ km s^{-1} Mpc^{-1}, which we adopt as the result for this paper.

4. COMPARISON WITH RIESS ET AL. (2011)

In this section, we compare our results with those of Riess et al. (2011). In their calibration of the SN Ia distance scale, they consider three routes to calibrating the Cepheid distance scale: (1) through the maser galaxy, NGC 4258 (2) through the Milky Way parallax sample of Benedict et al. (2007), and (3) through the LMC. Their second and third paths include an additional allowance in the uncertainty for possible differences in the zero points of the photometry transferring from their WFC3 photometric system to the ground-based photometric calibration of the parallax sample. We can compare our results most directly with Riess et al. by comparing our relative LMC distance moduli (their path 3) and establishing a 3.6 μm calibration for the SN Ia relative distance scale. Riess et al. adopt a distance modulus to the LMC of 18.486 ± 0.076 based on the Cepheid H-band sample of Persson et al. (2004), and measurements of eclipsing binaries. Their uncertainty includes the instrumental zero points, filter transmission functions, etc. Adopting this distance to the LMC, they found $H_0 = 74.4 \pm 2.5$ km s^{-1} Mpc^{-1}. Combining the zero points from the Milky Way, LMC, and NGC 4258, they adopt a final value of $H_0 = 73.8 \pm 2.3$ km s^{-1} Mpc^{-1}.

The LMC distance adopted by Riess et al. (2011) is in very good agreement with our new distance to the LMC, which is based entirely on new and completely independent 3.6 μm Milky Way data from Monson et al. (2012) and LMC data from Scowcroft et al. (2011, 2012). The Riess et al. (2011) H_0 calibration makes use of a larger set of supernova data for which the total statistical uncertainties in the Hubble diagram amount to 2.1%. The excellent agreement of the new *Spitzer* calibration of H_0 with that of Riess et al. provides an independent check on both the value of and the current systematic uncertainties in H_0.

5. COMPARISON OF MEASUREMENTS OF THE DISTANCE TO THE LMC

Benedict et al. (2007) derived a K-band true distance modulus to the LMC of 18.48 ± 0.04 mag (their Table 15), based on their Milky Way calibration applied to the near-infrared data of Persson et al. (2004). Riess et al. (2011) review the eclipsing-binary data used to derive geometric distances to the LMC and, as noted above, quote an averaged value of 18.486 ± 0.065 mag. Applying the Riess et al. (2009) H-band Milky Way calibration to the Persson et al. (2004) data gives a true H-band distance modulus to the LMC of 18.49 mag (corrected for $E(B - V) = 0.10$ mag). As pointed out by Benedict et al. (2007), this tight correspondence of distance moduli for different wavelengths and in comparison with a geometric distance determination suggests again that any metallicity effect at long wavelengths is small.

Recently, Walker (2011) has reviewed the status of determinations of the distance to the LMC using five independent distance indicators including Cepheids, RR Lyrae stars, Eclipsing Binaries, Red Variables, and Red Clump stars. These various methods yield an average distance modulus to the LMC of 18.48 with a full range of 0.1 mag, i.e., $\sigma \sim \pm 1.5\%$. Overall, the agreement with the value obtained in this study is excellent.

6. COSMOLOGICAL IMPLICATIONS

Given a value of H_0 accurate to $\sim \pm 3\%$, what constraints can we place on cosmological parameters? Of particular interest in the current era of dark energy missions is the dark energy

equation of state, w_0. As discussed earlier, within the anisotropy spectrum for cosmic microwave background fluctuations there exist strong degeneracies between w_0 and H_0 (e.g., Efstathiou & Bond 1999; Hu 2005). An increase in the accuracy of H_0 therefore provides a direct means of breaking this degeneracy and improving the limits on w_0 from current and future CMB anisotropy experiments (e.g., *WMAP* and *Planck*).

No single experiment can constrain all of the degrees of freedom describing the current cosmological model. In order to make progress, we therefore must restrict our parameter space (e.g., assuming a flat universe ($\Omega_k = 0$) or $w_0 = $ constant). To open up the parameter space requires combining different sets of experimental data, each with their own errors and systematics. Fortunately, Bayesian inference offers a straightforward way to combine experimental data, either through the computation of the likelihoods given each set of data or by imposing priors. In the case of the CHP, our constraints on H_0, being derived from the local distance scale, are independent of the other cosmological parameters and our data can therefore be incorporated as a simple Gaussian prior, centered on $H_0 = 74.3$ km s^{-1} Mpc^{-1} with a width $\sigma = 2.1$ km s^{-1} Mpc^{-1}.

To investigate the constraints on w_0, we use the Markov Chain Monte Carlo (MCMC) code COSMOMC developed by Lewis & Bridle (2002).[4] To incorporate our CHP prior, we modified COSMOMC to include the run-time prior add-on written by Adam Mantz.[5] When incorporating data from SNe Ia, we use further modifications by Alex Conley.[6]

We begin by combining our result with the WMAP7 cosmic microwave background anisotropy measurements (Komatsu et al. 2011). We assume a flat universe ($\Omega_k = 0$) and a dark energy equation of state that does not evolve with time ($w_a = 0$). Given these constraints, the resulting best-fit values for the equation-of-state parameter are $w_0 = -1.09 \pm 0.10$. In Figure 4(a), we show 1σ and 2σ confidence regions in the H_0/w_0 plane using both the CHP constraint on H_0 (blue curve) and the constraint from F01 (red curve). By way of comparison, the most recent results combining SNe Ia, WMAP7, and baryon acoustic oscillations (BAOs) under the same constraints ($\Omega_k = 0$ and $w_a = 0$) give $w_0 = -0.997^{+0.077}_{-0.082}$ (Amanullah et al. 2010). Both results are compatible with a simple cosmological constant. It should be noted that because the predictive power of SNe Ia is in the measurement of the curvature of the Hubble diagram (and not its zero point), any constraints on dark energy derived from SNe Ia are insensitive to improvements in the accuracy of H_0.

We next incorporate results from BAOs. Unlike SNe Ia, BAO experiments lack a low-redshift measurement, and in a combined analysis of this type, the results are therefore constrained by an accurate value of H_0. Keeping the same constraints as before ($\Omega_k = 0$ and $w_a = 0$) and adding in the data from Reid et al. (2010), we find $w_0 = -1.1 \pm 0.10$. We also find that the posterior distribution of H_0 has been shifted down to $H_0 = 72.7 \pm 2.0$ km s^{-1} Mpc^{-1}. The earlier, broader prior from F01 would bring the value of H_0 down even lower to $H_0 = 66.0^{+4.1}_{-4.5}$ km s^{-1} Mpc^{-1} (see Figure 4(b)), resulting in a difference between the value of H_0 from CMB+BAO alone and that derived from the CHP. Pushing the data a little further, we can remove the constraint for a flat universe. Again, keeping $w_a = 0$ and combining WMAP7 and BAO, the constraints on w_0 are reduced considerably, resulting in a best-fit value of $w_0 = -1.38 \pm 0.24$, which is inconsistent with a cosmological
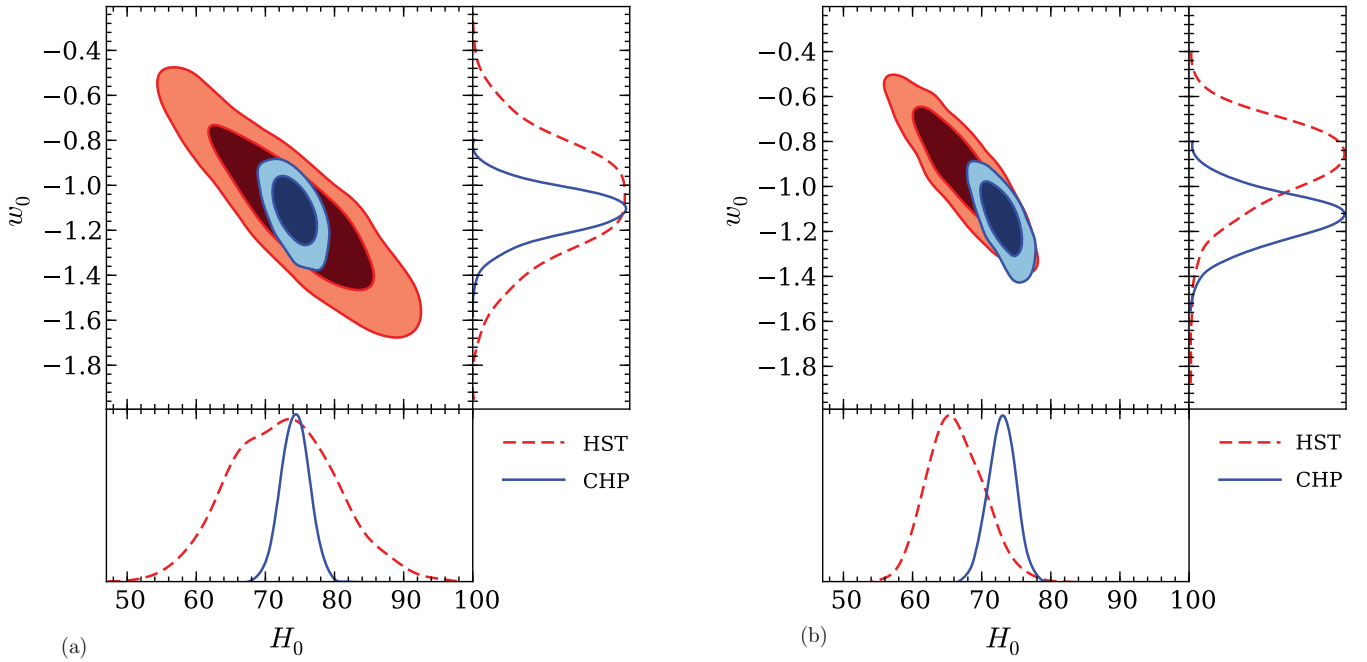

Figure 4. Two-dimensional confidence plots of the equation-of-state parameter w_0 and the Hubble constant H_0 using (a) the WMAP7 data alone and (b) WMAP7 and BAO data combined, and assuming $\Omega_k = 0$, $w_a = 0$, and $N_{\rm eff} = 3.046$. The red contours show the results using the prior from F01, while the blue contours show the results using the prior from this paper (labeled CHP). The right and bottom panels show the one-dimensional marginalized posterior probability distributions (PPDs) for w_0 and H_0, respectively. The F01 PPD is plotted as red dashed lines, the CHP PPD is plotted as blue solid lines.
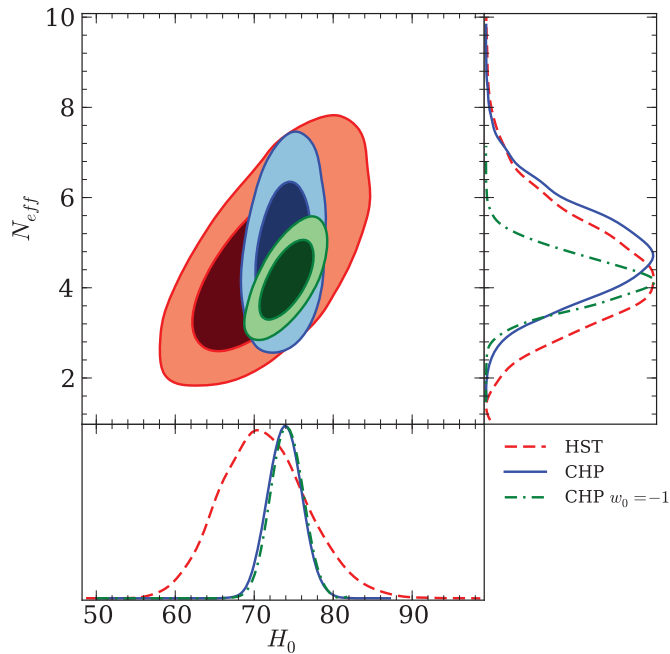

Figure 5. Two-dimensional confidence plot of the effective number of neutrinos $N_{\rm eff}$ and the Hubble constant H_0 using the WMAP7 data and BAO data combined and assuming $\Omega_k = 0$, $w_a = 0$. The red contours show the results using the prior from F01, the blue contours show the results using the prior from this paper (labeled CHP), and the green contours show the results using the CHP prior and assuming $w_0 = -1$. The right and bottom panels show the one-dimensional marginalized posterior probability distributions (PPDs) for $N_{\rm eff}$ and H_0, respectively. The F01 PPD is plotted as red dashed lines, the CHP PPD is plotted as blue solid lines, and the CHP+$w_0 = 1$ PPD is plotted as a green dash-dotted line.
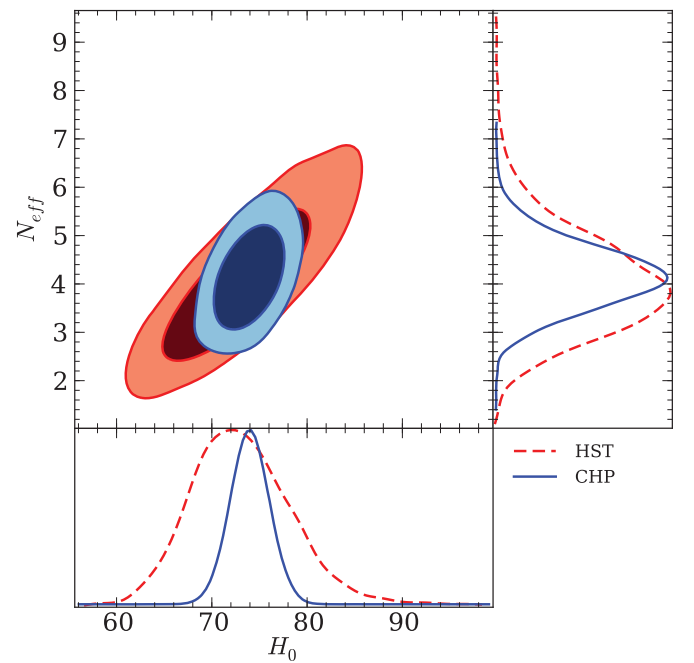
Figure 6. Two-dimensional confidence plot of the effective number of neutrinos $N_{\rm eff}$ and the Hubble constant H_0 using the WMAP7, BAO, and SN Ia data combined and assuming $w_a = 0$. The red contours show the results using the prior from F01, and the blue contours show the results using the prior from this paper (labeled CHP). The right and bottom panels show the one-dimensional marginalized posterior probability distributions (PPDs) for $N_{\rm eff}$ and H_0, respectively. The F01 PPD is plotted as red dashed lines and the CHP PPD is plotted as blue solid lines.

constant at about 1.5σ. The discrepancy between the prior and posterior values of H_0 is reduced somewhat, owing to the increased degrees of freedom in this model. The resulting constraint on the curvature parameter is $\Omega_k = -0.013 \pm 0.007$, favoring a flat universe at almost 2σ.

We also explore increasing the effective number of relativistic particles or number of neutrino species, ($N_{\rm eff}$). We do not consider limits on neutrino masses here. There is a large body of literature on the subject of constraints on neutrino physics (masses and numbers of particles) from cosmology (see Ma & Bertschinger 1995; Dolgov 2002; Lesgourgues & Pastor 2006). During the radiation era, neutrinos play a significant role in the cosmological expansion. Neutrinos also affect the growth of structure and alter the amplitudes of the peaks in the cosmic microwave background spectrum, both suppressing and shifting the positions of the acoustic CMB peaks. The effective number of neutrino species in the standard model of particle physics is $N_{\rm eff} = 3.046$. The presence of extra relativistic particle species can lead to measurable effects in the CMB spectrum (e.g., Dunkley et al. 2009; Komatsu et al. 2009, 2011).

Assuming that the extra relativistic particles are massless neutrinos, their density can be related to the density of photons through $\rho_\nu = 0.2271 N_{\rm eff} \rho_\gamma$ (Komatsu et al. 2009). This then modifies the evolution of the Hubble parameter, $H(z)$, by replacing the standard photon density parameter with $\Omega'_\gamma = \Omega_\gamma (1 + 0.2271 N_{\rm eff})$. Figure 5 illustrates the constraints on the number of neutrino species, adopting the Komatsu et al. (2009) model and combining the CHP H_0 value with WMAP7 and BAO data. To begin, we assume a flat universe. We find $N_{\rm eff} = 4.8 \pm 1.0$. In this case, the agreement in the value of H_0 is improved, but now the equation-of-state parameter shifts to a higher value: $w_0 = -0.85 \pm 0.14$. If we further restrict the model to a pure cosmological constant ($w_0 = -1$), then the constraints tighten to $N_{\rm eff} = 4.1 \pm 0.5$, differing by 2σ from the standard value.

In order to investigate the case where both Ω_k and $N_{\rm eff}$ are free to vary, we need to incorporate an additional independent data set. We use the SN Ia data from Sullivan et al. (2011), consisting of the SNLS 3 year sample, the SDSSII SN sample, the high-z sample from Riess et al. (2007), and several low-redshift samples from the literature. As we mentioned earlier, supernovae have the advantage that they can be observed at low redshift and therefore do not require H_0 to constrain w_0. Nevertheless, current observations of supernovae extend only to redshift $z = 1.4$ and therefore do not probe the epoch when radiation was more important. With this increased data set, we now relax both restrictions on Ω_k and $N_{\rm eff}$. Figure 6 shows the combined results of WMAP7, SN Ia, and BAO. Once again, the red contours show the earlier constraints from F01 and the blue contours show the constraints using the CHP results. The CHP data do not improve the constraints on w_0 in this scenario, yet they still improve the constraints on the number of neutrinos: $N_{\rm eff} = 4.13 \pm 0.67$. A summary of these cosmological constraints is included in Table 2.

These MCMC calculations, incorporating our CHP H_0 prior and combining with the WMAP7 data, strongly favor a universe with $w_0 \sim -1$. Adding in additional data from BAO and SNe Ia, they are consistent at the 2σ level with an additional neutrino species. Other recent studies have obtained results very similar to those obtained here (e.g., Dunkley et al. 2009; Reid et al. 2010; Riess et al. 2011; Komatsu et al. 2011; Mehta et al. 2012; Keisler et al. 2011; Benson et al. 2011). Given the number of degrees of freedom, and real degeneracies that exist among the parameters, caution should be exercised in interpreting 2σ results. Future data (e.g., from *Planck*) should settle the question of the number of neutrino species definitively.

7. DISCUSSION AND CONCLUSIONS

As we saw in Figure 3, we have graphically summarized the decrease in each of the systematic uncertainties, comparing the *HST Key Project* and the CHP. There are four key systematic improvements to the Cepheid distance scale that have occurred in the decade separating this study and the *HST Key Project*.

First, the *Spitzer* 3.6 μm data provide a zero point that is about an order of magnitude less sensitive to total line-of-sight extinction than the optical bands used for the *Key Project*. Systematic uncertainties in the reddening corrections (and uncertainties in the extinction law itself) are virtually eliminated in moving to the mid-IR.

Second, longer-wavelength data are theoretically predicted (e.g., Marconi et al. 2005; Romaniello et al. 2008) and empirically demonstrated (Freedman & Madore 2010; Freedman et al. 2011; Riess et al. 2011; this paper) to be less sensitive to metallicity. Moreover, the Milky Way Cepheid sample (now setting the zero point) has a metallicity more comparable to those of the majority of the *HST Key Project* spiral galaxies, thereby eliminating the bulk of the systematic uncertainty involved in previously using the (lower-metallicity) LMC Cepheids for the zero-point calibration.

Third, there are now direct parallax measurements for a representative sample of Milky Way Cepheids to define geometrically the absolute zero point of the Leavitt relation (Benedict et al. 2007). This new *Spitzer* Galactic trigonometric zero point eliminates the long-standing dependence on the distance to the LMC. Long-period LMC Cepheids simply define the slope and width of the 3.6 μm Leavitt law. In addition, independent geometric methods for measuring the distance to the LMC agree with the Cepheid calibration to within 1.5% rms in distance, providing an external check on this new calibration.

Fourth, and independently of the CHP, new near-infrared Cepheid distances to galaxies containing SNe Ia (Riess et al. 2011), as well as larger samples of more distant supernovae (Hicken et al. 2009), have become available.

Based on our analysis of the *Spitzer* data available to date, combined with data from the *Hubble Key Project*, we find $H_0 = 74.3 \pm 1.5$ (statistical) ± 2.1 (systematic) km s^{-1} Mpc^{-1}. This value of H_0 is in excellent agreement with that of the *Key Project*, as well as that of Riess et al. (2011). Combining this result with constraints from WMAP7 alone yields a value for the dark energy equation of state of $w_0 = -1.09 \pm 0.10$. Further combining BAO and SNe Ia data, and relaxing the restriction on the numbers of neutrino species results in a model with $w_0 = -1.08 \pm 0.10$ and $N_{\rm eff} = 4.13 \pm 0.67$. These data are compatible with, but do not require the presence of an additional neutrino species.

The dominant source of systematic uncertainty in our new value of H_0 is the zero-point uncertainty in the Cepheid period–luminosity relation, currently limited by the small numbers of long-period Cepheids having trigonometric parallaxes. Nevertheless, this uncertainty is now more than a factor of three smaller than the zero-point uncertainty for the *Key Project*.

As outlined in F11, as part of the CHP, we have also already observed Cepheids at 3.6 μm in a sample of nearby Local Group galaxies and beyond; we are undertaking several metallicity tests of the Leavitt relation at 3.6 μm; we are measuring a Cepheid distance to the maser galaxy, NGC 4258 at 3.6 μm;

Table 2
Constraints on Cosmological Parameters

Data Set/Priors	Ω_k	Ω_m	w_0	$N_{\rm eff}$
H_0+WMAP7 ($\Omega_k = 0$, $N_{\rm eff} = 3$)	...	0.246 ± 0.016	-1.09 ± 0.10	...
H_0+WMAP7+BAO ($\Omega_k = 0$, $N_{\rm eff} = 3$)	...	0.263 ± 0.015	-1.11 ± 0.11	...
H_0+WMAP7+BAO ($N_{\rm eff} = 3$)	-0.013 ± 0.008	0.253 ± 0.016	-1.38 ± 0.24	...
H_0+WMAP7+BAO ($\Omega_k = 0$)	...	0.296 ± 0.027	-0.88 ± 0.15	4.8 ± 1.0
H_0+WMAP7+BAO+SNLS	-0.007 ± 0.007	0.278 ± 0.018	-1.08 ± 0.10	4.13 ± 0.67

Notes. The values quoted are medians of the PPD. The errors are computed by finding the interval over which 68% of the probability is contained.

and we are calibrating the Tully–Fisher relation at mid-infrared wavelengths. Future improvements in the Cepheid zero point will come with the launch of *Gaia*, and an increased sample of Milky Way Cepheids and RR Lyrae stars with accurate parallaxes, which are needed to better define the zero point of the Leavitt relation. Having a value of H_0 with an externally well tested and robust total error budget of less than 2% appears feasible within the next decade.

Note added in proof. As noted in Section 2.2, the dispersion in the tilt-corrected LMC Leavitt law at 3.6 μm is ±0.100 mag. The dispersion in the Milky Way HST parallax sample is ±0.104 mag, consistent with that observed for the LMC. However, we also note that the error bars quoted for the Benedict et al. observations are larger than would be expected for this observed dispersion. More accurate parallaxes and a larger parallax sample from Gaia observations will be needed to understand the reason for this discrepancy. At present, we adopt the dispersion as measured, and note the good agreement between the Milky Way sample and that measured for the larger and statistically more well-defined sample of the LMC.

APPENDIX

CROWDING ERRORS

We present here a quantitative discussion of the effects of crowding on the errors in magnitudes and colors of Cepheids as used to determine distance in the *HST Key Project* (Freedman et al. 2001). The *Key Project* galaxy fields are dominated by a blue plume of high-mass, high-luminosity O and B supergiants, which are the longer-lived progenitors of the Cepheid variables. The blue plume stars are therefore the most likely objects to be crowding the Cepheids and contaminating their photometry.

Figure 7 illustrates the effects of the contamination of a Cepheid by blue main-sequence stars. The uncontaminated Cepheid is given a fiducial magnitude of $V = 0.0$ mag and a typical Cepheid color of $(V - I) = 1.00$ mag. A sequence of progressively brighter main-sequence stars, each having $(V - I) = 0.2$ mag, was then sequentially added to the light
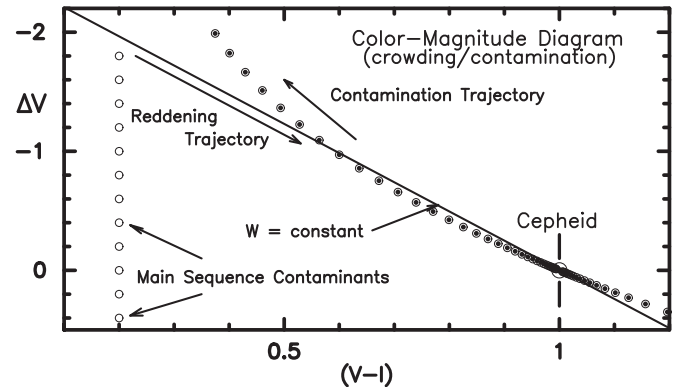

Figure 7. Numerical simulation of the effects of the contamination of a Cepheid by an excess of blue main-sequence stars under the point-spread function (artificially brightening the Cepheid) or in the annulus defining the sky (thereby artificially dimming the Cepheid). The uncontaminated Cepheid, shown by the large circle in the lower right of the panel, is set to have fiducial magnitudes and colors of $V = 0.0$ mag and $(V - I) = 1.00$ mag. A sequence of progressively brighter main-sequence stars (shown as open circles to the left of the panel (plotted vertically at $(V - I) = 0.2$ mag) is sequentially added to the light of the Cepheid and the combined light of the two is then plotted as a circled dot. The solid line passing through the Cepheid and up and to the left is a line of constant W, the reddening-free magnitude used by the *Key Project*.

of the Cepheid. The combined light of the two is plotted as circled dots progressively making the contaminated Cepheid appear brighter and bluer. The contaminated Cepheid appears fainter and redder if an uncorrected statistical excess of blue-plume light was contained in the sky aperture.

"Fainter and redder" has the same sense of direction in the color–magnitude diagram as extinction/reddening. For the *Key Project*, reddening was accounted for by producing a Wesenheit reddening-free magnitude $W = V - R \times (V - I)$, where R is the ratio of total-to-selective absorption such that $R = A_V/E(V - I)$, where A_V is the extinction and $E(V - I)$ is the reddening, and R in this case has the independently determined value of 2.45. A line of constant W passing through our sample Cepheid is shown as the solid line crossing the color–magnitude diagram diagonally from upper left to lower right. This line also closely tracks the contamination trajectory defined by the circled dots.

Quantitatively, for contaminating stars up to 1.8 mag brighter than the Cepheids, the contaminated Cepheids are only at most 0.06 mag in V away from the line of constant W. In fact, the average difference in W is only 0.03 mag over the range where the V magnitude increases by a full magnitude due to contamination. At low levels of contamination, this effect is smaller by a factor of four. For the illustrative purposes here, we have not modeled the luminosity function of the blue plume stars. We note, however, that the slope of the luminosity function

is such that contamination by brighter stars is statistically less likely than for fainter stars. These results are quantitatively consistent with the artificial star experiments of Ferrarese et al. (2000), who concluded that the effects of crowding in the *Key Project* fields were less than 0.02 mag or 1% in distance. Consequently, as discussed in Section 3 and shown in Figure 3, we have adopted a current uncertainty of 1% for this effect.

REFERENCES

Allende-Prieto, C., Lambert, D. L., & Asplund, M. 2001, ApJ, 556, L63
Amanullah, R., Lidman, C., Rubin, D., et al. 2010, ApJ, 716, 712
Benedict, G. F., McArthur, B. E., Feast, M. W., et al. 2007, AJ, 133, 1810
Benson, B. A., de Haan, T., Dudley, J. P., et al. 2011, arXiv:1112.5435v1
Dolgov, A. D. 2002, Phys. Rep., 370, 333
Dunkley, J., Komatsu, E., Nolta, M. R., et al. 2009, ApJS, 180, 306
Efstathiou, G., & Bond, J. R. 1999, MNRAS, 304, 75
Fazio, G. G., Hora, J. L., Allen, L. E., et al. 2004, ApJS, 154, 10
Ferrarese, L., Silbermann, N. A., Mould, J. R., et al. 2000, PASP, 112, 177
Freedman, W. L., & Madore, B. F. 2010, ARA&A, 48, 673
Freedman, W. L., Madore, B. F., Gibson, B. K., et al. 2001, ApJ, 553, 47 (F01)
Freedman, W. L., Madore, B. F., Scowcroft, V., et al. 2011, AJ, 142, 192 (F11)
Hicken, M., Wood-Vasey, W. M., Blondin, S., et al. 2009, ApJ, 700, 1097
Hu, W. 2005, in ASP Conf. Ser. 339, Observing Dark Energy, ed. S. C. Wolff & T. R. Lauer (San Francisco, CA: ASP), 215
Keisler, R., Reichardt, C. L., Aird, K. A., et al. 2011, arXiv:1105.3182
Komatsu, E., Dunkley, J., Nolta, M. R., et al. 2009, ApJS, 180, 330
Komatsu, E., Smith, K. M., Dunkley, J., et al. 2011, ApJS, 192, 18
Lesgourgues, J., & Pastor, S. 2006, Phys. Rep., 429, 307
Lewis, A., & Bridle, S. 2002, Phys. Rev. D, 66, 103511
Ma, C.-P., & Bertschinger, E. 1995, ApJ, 455, 7
Marconi, M., Musella, I., & Fiorentino, G. 2005, ApJ, 632, 590
Mehta, K. T., Cuesta, A. J., & Xu, X. 2012, arXiv:1202.0092
Meixner, M., Gordon, K. D., Indebetouw, R., et al. 2006, AJ, 132, 2268
Monson, A., Freedman, W. L., Madore, B. F., et al. 2012, ApJ, submitted
Persson, S. E., Madore, B. F., Krzeminski, W., et al. 2004, AJ, 128, 2239
Reid, B. A., Percival, W. J., Eisenstein, D. J., et al. 2010, MNRAS, 404, 60
Riess, A. G., Macri, L., Casertano, S., et al. 2009, ApJ, 699, 539
Riess, A. G., Macri, L., Casertano, S., et al. 2011, ApJ, 730, 119
Riess, A. G., Strolger, L.-G., Casertano, S., et al. 2007, ApJ, 659, 98
Romaniello, M., Primas, F., Mottini, M., et al. 2008, A&A, 488, 731
Sandage, A., Reindl, B., & Tammann, G. A. 2010, ApJ, 714, 1441
Scowcroft, V., Freedman, W. L., Madore, B. F., et al. 2011, ApJ, 743, 76
Scowcroft, V., Freedman, W. L., Madore, B. F., et al. 2012, ApJ, 747, 84
Stetson, P. B. 1998, PASP, 110, 1448
Sullivan, M., Guy, J., Conley, A., et al. 2011, ApJ, 737, 102
Suyu, S. H., Treu, T., Blandford, R. D., et al. 2012, arXiv:1202.4459
Turnbull, S. J., Hudson, M. J., Feldman, H. A., et al. 2011, MNRAS, 420, 447
Turner, E. L., Cen, R., & Ostriker, J. P. 1992, AJ, 103, 1427
Walker, A. R. 2011, Ap&SS (arXiv:1112.3171)
Werner, M. W., Roellig, T. L., Low, F. J., et al. 2004, ApJS, 154, 1
Windmark, F., Lindegren, L., & Hobbs, D. 2011, A&A, 530, A76